Anal. Chem. 1990, 62, 447–452

Electrochemical Behavior of Reversible Redox Species at Interdigitated Array Electrodes with Different Geometries: Consideration of Redox Cycling and Collection Efficiency

Osamu Niwa,* Masao Morita, and Hisao Tabei

NTT Basic Research Laboratories, Nippon Telegraph and Telephone Corporation, Tokai, Ibaraki 319-11, Japan

Interdigitated array (IDA) electrodes with different geometric parameters have been fabricated by a lithographic technique and applied to cyclic voltammetric and chronoamperometric measurements of reversible redox species. The collection efficiency is dependent on the average diffusion length of $W_e/4$ + gap, where W_e is the band electrode width in the IDA. The number of redox cycles rapidly increases by decreasing $W_e/4$ + gap and is closely related to collection efficiency. The difference in species diffusion constant had little effect on the collection efficiency and redox cycling. The high redox cycling and collection efficiency of the IDA's allowed electrochemical measurements to be highly sensitive (10 nmol/dm³), with a high signal to noise ratio and a wide dynamic range (10 nmol/dm³ to 1 mmol/dm³). Chronoamperometric measurement has been performed in a four-electrode configuration where step potential was applied to the generator electrode and constant potential was applied to the collector electrode in the IDA. The generator current reached steady state within a hundred milliseconds and the collector current was not affected by charging. With the IDA, fast sweep cyclic voltammetry with no observable charging current has been also demonstrated.

Microelectrodes are of interest for several reasons such as small *iR* drop, fast establishment of steady-state mass transfer, and small capacitive charging currents. A variety of microelectrodes have been constructed and studied both experimentally and theoretically (*1–3*). Possible applications include fast cyclic voltammetry (*4–7*), electrochemical measurements in vivo or in low conductive media (*8–10*), and chemical sensing (*11–14*). Micro fabrication techniques can be applied to produce a variety of sizes and/or shapes of microelectrodes compared to the conventional fabrication techniques of sealing carbon or metal fibers in a glass capillary tube or sealing metal foil between two glass plates (*15*). It also allows microelectrodes of the same size and of any shape to be produced without difficulty. Lithographically fabricated microelectrodes have attracted much attention as ion-selective field effect transistors (*11*, *16*) or electrochemical diodes and transistors (*17–24*).

Interdigitated array (IDA) electrodes are particularly interesting, because their geometric differences from conventional electrodes result in specific electrochemical behavior (*25*). Nonplanar diffusion to each microband electrode in IDA gives rise to quasi-steady-state currents for moderate sweep rates with a reversible redox couple. The species generated at one band electrode may be collected at adjacent band electrodes when the potential is set to a level at which a reverse reaction can occur. This type of experiment has been carried out with rotating ring–disk electrodes (RRDE) and paired microband electrodes with a small gap (*26*, *27*). Collection efficiency can be defined as the ratio of currents at the generator and collector electrodes. An important feature of IDA compared to RRDE is that the collected species will be electrolyzed at the collector electrodes and then diffuse back to the generator electrodes (*25*). This redox cycling or "feedback effect" (*26*) makes the currents of both the generator and collector electrodes larger.

Another feature is that the collector electrodes are held at a constant potential. This allows us to measure faradaic currents without charging currents caused by potential change. The fast sweep cyclic voltammogram is not distorted by the increased charging current. The collector electrode currents directly reveal the diffusion characteristics between the generator and collector electrodes (*28*, *29*).

Aoki and we discussed reversible diffusion-controlled currents of redox soluble species at IDA electrodes under steady-state conditions (*30*). In this paper, the relationship between the geometric configuration and the electrochemical characterization of IDA's, particularly collection efficiency and redox cycles are described. High redox cycling and collection efficiency of IDA's allow electrochemical measurements to be highly sensitive, with a high signal to noise ratio and a wide dynamic range. We also demonstrate fast sweep cyclic voltammetry without a charging current by using IDA.

EXPERIMENTAL SECTION

Electrodes. Interdigitated array (IDA) electrodes were fabricated on thermally oxidized silicon wafers. Platinum electrodes were formed by sputter deposition and the lift-off technique as described elsewhere (*30*, *31*). The submicrometer IDA electrodes were fabricated with a combination of electron beam lithography and photolithography. The platinum pad and the lead pattern were formed by photolithography and the lift off technique. Then a-PMMA/S-MAC (Daikin Manufacturing Co., Osaka) bilayer electron beam positive resist was spin coated on to the wafers exposed with ELS-5000 (Elionix, Japan) electron beam exposure, and developed. Both wafers with micrometer and submicrometer patterns were then spin-coated with spin-on-glass (OCD Type-7, Tokyo Ohka Co.), and baked at 430 °C for 30 min. The final thickness of the spin-on-glass was 800 nm. An MP1400-27 (Shipley) positive photoresist pattern was formed on the wafer and used as an etching mask. The silicon dioxide film made from the spin-on-glass was etched by DEM-451 reactive ion etching equipment (ANELVA, Tokyo) with tetrafluoromethane until the surfaces of the IDA electrode and pad were exposed. The photoresist remaining after etching was removed in the methyl ethyl ketone solution.

Each IDA cell was cut to a 1 × 2 cm rectangle and mounted on a custom-made connector to attach it to the electrochemical apparatus. The auxiliary electrode was a platinum wire. The reference electrode was an Ag/AgCl electrode.

The IDA used consists of two series of interdigitated microband electrodes, whose geometric parameters are summarized in Table I. Figure 1 shows an SEM photograph of an IDA with a 3-μm bandwidth and a 2-μm gap.

Apparatus and Reagents. Electrochemical measurements were performed with a dual potentiostat, DPGS-3 (Nikko Keisoku, Atsugi, Japan) and HECS990 (Fuso, Japan), a digital memory oscilloscope, Model 4094B (Nicolet, Madison, WI), and a universal pulse programmer, Model 175 (Princeton Applied Research, Princeton, NJ).

The reagents were ferrocene, (ferrocenylmethyl)trimethylammonium bromide (aq-ferrocene), potassium ferrocyanide, ruthenium hexaamine, tetrabutylammonium tetrafluoroborate, potassium nitrate, and acetonitrile and were used as purchased.

Table I. Geometric Parameters and Collection Efficiencies for Various Redox Species of the IDA Electrodes[a]

IDA size				collection efficiency/%			
W_e/μm	gap/μm	length/mm	no. of bands	aq-ferrocene	ferrocene	ferrocyanide	$Ru(NH_3)_6$
0.75	0.75	1	135	99.5	99.1	98.5	98.9
1.0	1.0	1	100	100	98.7	98.8	98.1
1.5	1.5	1	100	100	98.5	97.9	97.8
3.0	2.0	2	50	99.3	98.0	98.3	95.9
5.0	2.0	2	50	96.2	96.1	95.7	95.4
10.0	2.0	2	25	93.5	93.7	93.0	95.0
3.0	5.0	2	50	94.6	94.2	94.7	92.2
5.0	5.0	2	50	92.8	93.6	91.5	91.6
10.0	5.0	2	25	90.0	90.1	89.3	91.9

[a] The composition of the solution is in Table II. Key: generator electrode, swept at 10 mV/s; collector electrode, −0.1 V [0 V for $Ru(NH_3)_6$].

Table II. Redox Species

name	concn, mmol/dm³	supporting electrolyte	solvent	diffusion constant, cm²/s
ferrocene	1.0	Bu_4NBF_4	CH_3CN	2.4×10^{-5}
aq-ferrocene[a]	1.0	KNO_3	H_2O	6.1×10^{-6}
ferrocyanide	1.0	KCl	H_2O	6.4×10^{-6}
Ru hexaamine	1.0	KNO_3	H_2O	7.1×10^{-6}

[a] (Ferrocenylmethyl)trimethylammonium bromide.

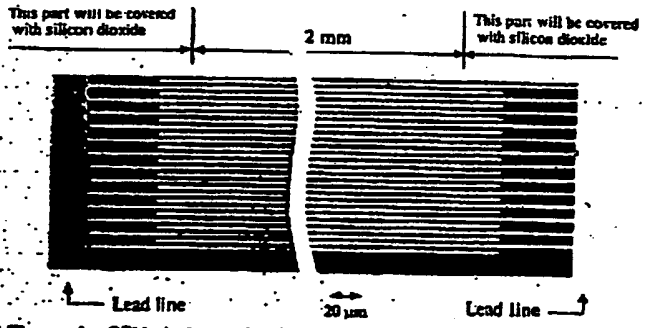

Figure 1. SEM photograph of part of Pt band pattern of IDA. The 3-μm width, 2-μm gap, 2 mm long IDA contains 50 bands on each sides. This picure was taken before the spin-on-glass coating. After spin-on-glass coating and etching, the lead lines are covered with silicon dioxide.

The redox species used are summarized in Table II with other parameters.

Procedure. Electrochemical measurements were carried out in 1 mmol/dm³ ferrocene acetonitrile solution or 1 mmol/dm³ ruthenium hexaamine, aq-ferrocene, or potassium ferrocyanide aqueous solutions purged with nitrogen in the usual three-electrode (open-circuit mode, one of the paired electrodes in the IDA was disconnected) or four-electrode (generation-collection mode) configuration. The resistance between IDA (gap, 2 μm) is more than 100 MΩ and about 7 MΩ at dry and wet (in H_2O) state, respectively. In measuring the cyclic voltammogram of ferrocene, aq-ferrocene and potassium ferrocyanide, the potential of the collector electrode was held at −0.1 V, and the generator electrode was swept between −0.1 and 0.7 V, at a sweep rate of 10–100 mV/s. In the case of ruthenium hexaamine, the collector was held at 0 V, and the generator was swept between 0 and −0.7 V. In order to obtain steady-state limiting currents in the open-circuit mode, it was necessary to decrease the sweep rate below 5 mV/s or 1 mV/s for ferrocene and other redox species, respectively.

In the generation-collection chronoamperometry of the ferrocene solution, the potential of the generator electrode was stepped up from 0 to 0.5 V, whereas the collector electrode was held at −0.1 V. The potential step current–time transients of both electrodes were stored in a digital memory oscilloscope and then recorded with a two-pen X-Y recorder.

The fast sweep rate cyclic voltammetry of ferrocene was carried out with a 3-μm width, 2 μm gap IDA electrode. The potential of the generator was swept from −0.3 to 0.75 V with rate of 10 V/s and that of the collector held at −0.1 V. The currents were stored in a digital memory oscilloscope and then recorded with a two-pen X-Y recorder.

RESULTS AND DISCUSSION

IDA Fabrication. The lithographic processing of IDA's is almost the same as previously described except for the use of electron beam lithography for fabricating the submicrometer IDA and spin-on-glass as an insulating layer. In the earlier work (*30*), a hard-baked photoresist was used as an insulator and failed occasionally when nonaqueous solvents were used. It was not sufficiently hard to resist scratching. The use of sputter-deposited silicon dioxide improved the reliability of the insulator (*31*), although this lengthened the insulator forming process.

The spin-on-glass consists mainly of aqueous silicate solution and can be spin-coated on a wafer like a photoresist coating. High temperature baking (430 °C) makes it cross-link and convert into silicon dioxide. Although the spin-on-glass insulator is inferior to the sputter-deposited one in hardness, it has sufficient quality as an insulator. It also has the advantage of providing smooth and uniform film, which improves the step coverage of the Pt electrodes at their edges.

Collection Efficiencies of IDA's with Different Geometric Parameters. The anodic and cathodic currents of ferrocene, aq-ferrocene, and potassium ferrocyanide at IDA electrodes are steady state, in which the potential of the cathode (collector electrode) was held at −0.1 V and the anode (generator electrode) was swept between −0.1 and 0.7 V at 10 mV/s.

Similar steady-state curves were obtained for ruthenium hexaamine, in which the potential of the collector electrode was held at 0 V vs Ag/AgCl and the generator electrode was swept between 0 and −0.7 V. These results are analogous to those obtained by rotating ring–disk measurement, but this steady-state condition was established only by mass transfer. The magnitude of the limiting currents at these IDA electrodes is increased by decreasing the bandwidth and gap in the IDA and corresponds to the theoretical value (*30*). The collection efficiency in the IDA, which can be calculated from the ratio between the generator and the collector currents, is increased by decreasing the electrode size and approaches unity. Table I also shows the collection efficiency of the IDA with various geometric parameters. Bard et al. (*27*) reported that the collection efficiency of a generator with two collector band electrodes (three microband electrode configuration) was strongly dependent on the gap, and was expressed as the following equation, when the generator and collector electrodes are the same size:

$$\Phi_{ss} = 0.095 + 0.33 \log \varphi_{gap} - 0.035 (\log \varphi_{gap})^2 \quad (1)$$

$$\varphi_{gap} = 4Dt/gap^2$$

where Φ_{ss} is the collection efficiency and t is the time. The

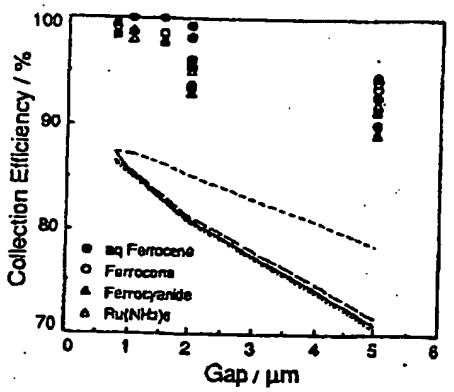

Figure 2. Collection efficiencies at the IDA electrodes compared with those resulting from eq 1, which is for one generator with two flanking collector microband electrodes (28). The composition of the solution is in Table II. Key: (- - -) aq-ferrocene; (- - -) ferrocene; (—) ferrocyanide; (- -) ruthenium hexaamine.

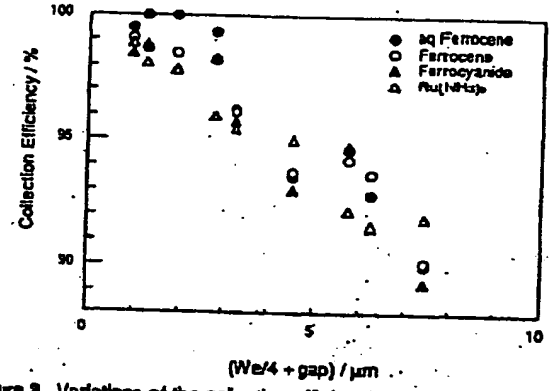

Figure 3. Variations of the collection efficiencies at the IDA electrodes as a function of the average diffusion length. The composition of the solution is in Table II.

collection efficiencies in the IDA were compared with theoretical values from eq 1.

Figure 2 shows a comparison of the collection efficiency in the IDA with the theoretical results (from eq 1). There are three main differences in the collection efficiency of IDA and that of the three microband electrode configuration. First, the collection efficiency at the IDA electrodes varies by changing not only the gap but also the bandwidth and does not fit with the results of eq 1. Second, the collection efficiency in the IDA did not change for different redox species despite the large difference in diffusion coefficient between ferrocene ($D = 2.4 \times 10^{-5}$ cm^2/s) and other redox species ($D = (6–7.1) \times 10^{-6}$ cm^2/s). It suggests that the collection efficiency of the IDA was only influenced by geometric factors like that of RRDE, at least the region we measured. Finally, the collection efficiency in the IDA is much higher than that for three microband electrodes with the same gap, indicating that the alternative array structure could decrease the active species, which diffuse back into the bulk solution.

From the results of the chronoamperometry at the IDA as described in the later section, the good proportionality between the square root of the half-height time when the collector transient current is at 50% of its limiting current and $W_e/4$ + gap was obtained. This shows that the $W_e/4$ + gap could be used to represent the average diffusion length between the generator and collector electrodes.

Figure 3 shows the collection efficiencies of various redox species as a function of average diffusion length ($W_e/4$ + gap). It is increased by decreasing the average diffusion length, and the average error is small (about +1.6%, see Figure 3). This suggests that $W_e/4$ + gap could be the more suitable parameter from which to evaluate the geometry dependence of the collection efficiency at the IDA electrodes.

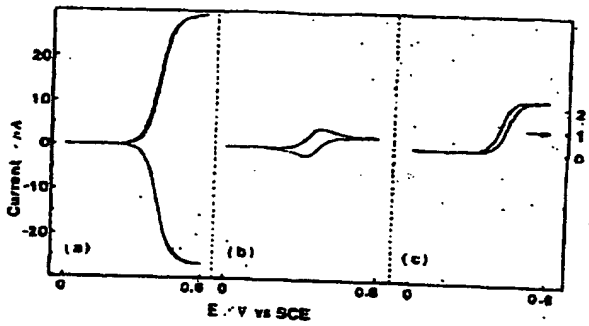

Figure 4. Cyclic voltammograms of 1 mmol/dm^3 ferrocene in 0.1 mol/dm^3 tetrabutylammonium tetrafluoroborate acetonitrile solution at a 3-μm width, 2-μm gap IDA with and without potentiostating the collector electrode: (a) generator electrode, swept at 100 mV/s; collector electrode, −0.1 V; (b) generator electrode, sweep at 100 mV/s; collector electrode, open circuit; (c) generator electrode, swept at 5 mV/s; collector electrode, open circuit.

Redox Cycling of IDA. The remarkable feature of IDA compared to RRDE is its high redox cycling which makes the currents of both the generator and collector electrodes larger. The steady-state waves of ferrocene with redox cycling (Figure 4a) change to a gentle decay of the current plateau as shown in Figure 4b, when the collector electrode is not potentiostated (open-circuit mode). A lower sweep rate of less than 5 mV/s produces a pseudo-steady-state wave, whose magnitude is much lower than those produced when using a collector electrode.

The redox cycles in the IDA can be calculated from the collection efficiency values. When the collection efficiency of the generator to collector electrode is Φ_1, and that when the generator and collector electrode are reversed is Φ_2, the number of ferrocene molecules which diffuse back to the generator electrode after reducing at the collector electrode can be expressed as $N\Phi_1\Phi_2$, where N is the number of ferrocene molecules oxidized per unit time at the generator electrode. So, the number of ferrocene molecules that diffuse into the bulk solution per cycle is $N - N\Phi_1\Phi_2$. Then, the number of redox cycles (Rc) is expressed by

$$Rc = N/N(1 - \Phi_1\Phi_2) = 1/(1 - \Phi_1\Phi_2) \quad (2)$$

In this experiment, Φ_1 and Φ_2 have the same value because the size of the generator and collector electrodes is the same. This method is useful to evaluate the redox cycles of IDA. However, the accuracy of the calculated redox cycles is governed by the experimental errors of the collection efficiency. Particularly, the calculated redox cycles are much scattered because the slight error in the collection efficiency was enhanced by eq 2, when the collection efficiency at the IDA is near unity.

We assumed the average number of redox cycles from the ratio of the limiting current of the generation–collection mode (i_g) to that of the open-circuit mode (i_o) and compared it with those calculated from eq 2. Figure 5 shows the redox cycles obtained from i_g/i_o compared with those obtained from eq 2. Although i_g/i_o is not the actual number of redox cycles, it is closely related with the number calculated from eq 2, when the $W_e/4$ + gap is more than 3.75 μm. Taking into account the i_g/i_o shows the good reproducibility, the difference between the calculated redox cycles and i_g/i_o may be caused by the fluctuation of the calculated results. These results indicate that i_g/i_o values could be substituted for the values from eq 2 to evaluate the actual number of redox cycles.

Figure 6 shows the average numbers of redox cycles (i_g/i_o) for various redox species as a function of the average diffusion length. The number of redox cycles rapidly increases by

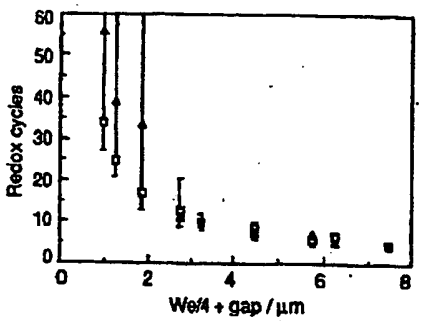

Figure 5. Ratio of the generator electrode current of ferrocene in generation–collection mode to that in open circuit mode (I_g/I_o) compared with redox cycles calculated with eq 2. The generators monitored in this experiment are 25 (bandwidth, 10 μm), 50 (bandwidth, 5 μm), and 100 (bandwidth, less than 1.5 μm): □, I_g/I_o; ▲, redox cycles by eq 2.

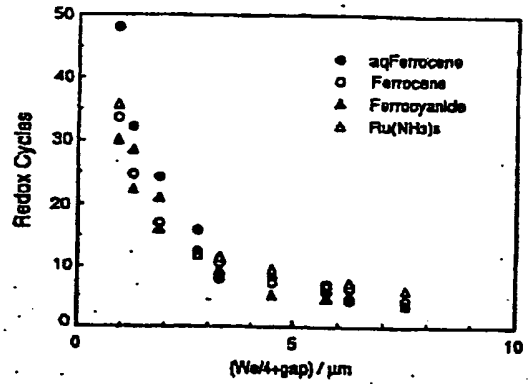

Figure 6. Variation of the redox cycles as a function of the average diffusion length. Redox cycles are the ratio of generator current, with the collector electrode open circuited, to generator current with the generator electrode on.

decreasing the average diffusion length and reaches more than 40 in the smaller IDA, which has a 0.75-μm bandwidth and gap. No clear difference in the number of redox cycles can be observed between the redox species.

On the other hand, the number of redox cycles in the three microband electrode configuration with a 1-μm gap is only 2.4 (feedback factor = 0.58 = 1 − 1/(redox cycling) (26), which is much smaller than that at an IDA electrode with the same gap. These differences in the number of redox cycles are caused by the following reasons. In the case of the three microband electrode, the generator electrode is located between two adjacent collector electrodes, whereas each collector electrode has only one adjacent generator electrode. Some active species reduced by the collector electrode could diffuse into the bulk solution from the electrode edge, furthest from the generator electrode.

In the case of the IDA electrode, the collection efficiency is almost same, when the generator and the collector electrodes are reversed. The redox species may escape in the bulk solution vertically or escape at the edge of the IDA electrode.

Concentration Dependence of Steady-State Currents. Since the voltammograms of the IDA electrode show a relatively high current density due to the high redox cycles, the sensitivity of the IDA was studied by changing the concentration of ferrocene.

Figure 7 shows the concentration dependence of the cathodic and anodic limiting current of ferrocene at an IDA electrode, whose bandwidth and gap are 3 and 2 μm, respectively. The anodic generator and cathodic collector currents were proportional to the concentration of ferrocene from 100 nmol/dm³ to 1 mmol/dm³ at a sweep rate of 10 mV/s. However, the quantitative generator anodic current

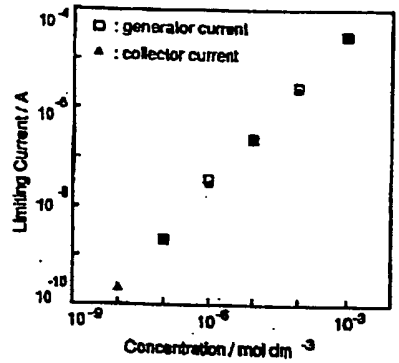

Figure 7. Concentration dependence of the cathodic and anodic limiting currents of ferrocene at an IDA with 3-μm width and 2-μm gap. The solvent is acetonitrile containing 10 nmol/dm³ to 1 mmol/dm³ ferrocene and 0.1 mol/dm³ tetraethylammonium tetrafluoroborate.

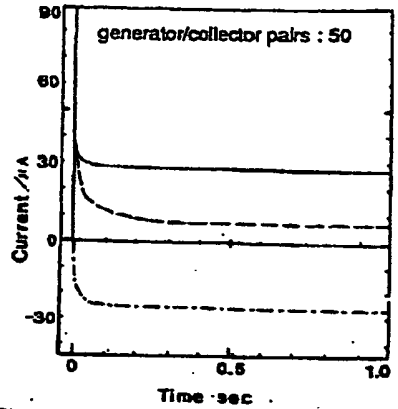

Figure 8. Chronoamperometric current–time curve (—) for potential step oxidation of 1 mmol/dm³ ferrocene in 0.1 mol/dm³ tetrabutylammonium tetrafluoroborate acetonitrile solution at a 3-μm width, 2-μm gap IDA electrode with 50 pairs of generator and collector electrodes. (– – –) represents the current of the collector electrode whose potential is held at −0.1 V. The dashed line shows an open-circuit mode current–time curve of the generator without potentiostating the collector electrode in IDA.

cannot be measured at a higher sweep rate and at a concentration of less than 100 nmol/dm³ due to the reduction of the signal to noise (S/N) ratio of the faradaic current to the charging current. On the other hand, the cathodic current was proportional to the concentration of ferrocene from 10 nmol/dm³ to 1 mmol/dm³ due to the absence of the charging current.

Recently, on conjunction with Aoki we (30) proposed steady-state equations for redox species at an IDA electrode and proved that the limiting current increases by decreasing the gap and bandwidth. Voltammograms of electroactive species with a lower concentration may be realized by using an IDA with a smaller gap and bandwidth. This is now under investigation.

Chronoamperometry of IDA. Current–time curves resulting from potential steps for IDA's in ferrocene acetonitrile solution were subjected to a detailed quantitative comparison with microband electrodes (32–34) and three microband electrodes (26). Figure 8 shows typical current–time curves from the generator (—) and the collector (– – –) of a 3-μm bandwidth, 2-μm gap IDA electrode. The dashed line in Figure 8 shows an open-circuit mode current–time curve of a generator with an unpotentiostated collector electrode in an IDA. The generator current of the generation–collection mode reaches steady-state within a hundred milliseconds. The steady-state response can be improved to 10 ms, when submicrometer IDA electrodes are used. The electrochemical response of the previously reported IDA electrode is not so

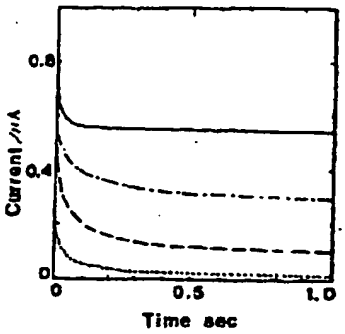

Figure 9. Chronoamperometric current–time curve for potential step oxidation of 1 mmol/dm³ ferrocene in 0.1 mol/dm³ tetrabutylammonium tetrafluoroborate acetonitrile solution at a 3-μm width, 2-μm gap IDA electrode: (—) represents the generator current in generator-collector mode, (– –) represents the open-circuit mode current. These currents are normalized by dividing the number of bands. (– – –) and (– · –) represent a theoretical current calculated from the Aoki–Coen equations, and the Cottrell equation, respectively.

rapid, because the bandwidth and gap are 50 μm (25). However, like the fast voltammogram of an ultramicroelectrode, our results for a submicrometer size IDA electrode show that a small IDA electrode can be applied to measure the electrochemical property of short lifetime species. Other remarkable characteristics of the IDA are that the current–time curve at the collector electrode consists of only faradaic current and is not affected by large noisy charging current. The transient region until the collection current becomes steady state reflected the redox species diffusion and the concentration gradient establishment.

The square root of the half-height time when the collector transient current is at 50% of its limiting current is proportional to the average diffusion length ($W_s/4$ + gap), and those plots fit well with the theoretical line of $d = (\pi Dt)^{1/2}$.

Aoki et al. (32, 33) derived the theoretical chronoamperometric response at a microband electrode as a function of the dimensionless electrolysis time θ, given by

$$\theta = Dt/w^2 \tag{3}$$

where t is the time in seconds and w is the electrode width in centimeters. The chronoamperometric curve is expressed

$$I/(bnFDC^*) = (\pi\theta)^{-1/2} + 0.97 - 1.10 \exp[-9.90/\ln(12.37\theta)] \tag{4}$$

for $\theta < 10^6$ ($t < 3.75 \times 10^6$ s for ferrocene, when W_s is 3 μm), where b is the length of the microband electrode and n, F, D, and C^* have their usual meanings.

Coen et al. (34) derived the following expression for the quasi-steady-state currents at a microband electrode:

$$I/(bnFDC^*) = 5.553/\ln(4\theta) - 6.791/(\ln(4\theta))^2 \tag{5}$$

Equation 3 holds for $\theta > 7.5$ ($t > 70$ ms for ferrocene in 10 μm bandwidth) and shows approximately the same results in longer time regions as eq 4. Figure 9 shows chronoamperometric current–time curves of both the generator–collector (—) and open-circuit (– –) mode for 3-μm bandwidth, 2-μm gap IDA's, in comparison with the Aoki–Coen equation (– · –) and the Cottrell equation (– – –). The currents in the IDA's are divided by the number of bands, normalizing in single microband currents. The current in the open-circuit mode shows a higher value than the Cottrellian, indicating that the diffusion profile is not longer planar. It is, however, much lower than the value calculated from the Aoki–Coen equation, because of the shielding effect (26). The current in the generator–collector mode shows a larger value than the Aoki–Coen equation, due to redox cycling. When the gap becomes 2–5 μm, the open-circuit mode current becomes larger because of a smaller shielding effect, but the generator–collection mode current becomes smaller because of less redox cycling.

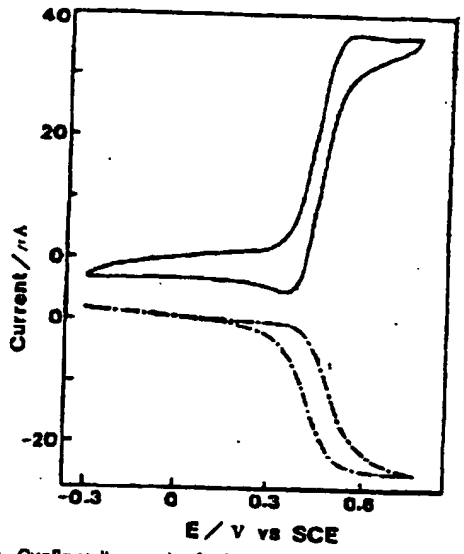

Figure 10. Cyclic voltammetry (—) of 1 mmol/dm³ ferrocene in 0.1 mol/dm³ tetrabutylammonium tetrafluoroborate acetonitrile solution at a 3-μm width, 2-μm gap IDA electrode. (– – –) represents the current of the collector electrode whose potential is held at −0.1 V.

Fast Sweep Cyclic Voltammetry. Important features of microelectrodes include their small double layer capacitance, which allows the exploration of extremely short electrolysis times and fast kinetic phenomena. On the other hand, the double layer charging current increases linearly with the sweep rate, whereas the faradaic current increases with the square root of the sweep rate at the high scan rate. Therefore, the signal becomes obscure in large charging current when the sweep rate becomes faster. Although computer digital subtraction between sample and blank solutions improves this problem (5), the essential low signal-to-noise ratio, signal distortion by the ohmic drop, and experiments on both sample and background still remain.

The collector current in the IDA is not affected by the charging current because the potential of the collector is held constant. Therefore, the no-charging current fast sweep rate cyclic voltammogram is expected. Figure 10 shows cyclic voltammetry in the generation–collection mode for ferrocene in a 3-μm width, 2-μm gap IDA. The sweep rate was 10 V/s, so that the voltammogram of the generator develops current peaks meaning that the radial diffusion profile dimension is approaching that of the electrode. On the other hand, the voltammogram of the collector maintained a steady-state response.

This effect was described 20 years ago in connection with thin-layer electrochemistry, but with no regard to IDA's. Hysteresis is caused by the delay between the generation and collection of redox species. The potential of the generator will be changed when the generated species diffuse and reach to the collector. The difference between cathodic and anodic waves in the collector voltammogram is about 80 mV. The sweep rate is 10 V/s; therefore the difference of 80 mV corresponds to 8 ms, which is close to the theoretical time in which the redox species crosses the gap.

ACKNOWLEDGMENT

We thank Professor K. Aoki for his helpful discussions and Dr. T. Tamamura for the fabrication of the IDA's by electron-beam lithography.

LITERATURE CITED

(1) Fleischmann, M.; Pons, S.; Rolison, D.; Schmidt, P. P. *Ultramicroelectrodes*; Datatech Science: Morganton, NC, 1987.

(2) Pons, S.; Fleischmann, M. *Anal. Chem.* **1987**, *59*, 1391A.
(3) Johnson, D. C.; Ryan, M. D.; Wilson, G. S. *Anal. Chem.* **1988**, *60*, 147R.
(4) Howell, J. O; Wightman, R. M. *Anal. Chem.* **1984**, *56*, 524.
(5) Howell, J. O.; Wightman, R. M. *J. Phys. Chem.* **1984**, *88*, 3915.
(6) Andrieux, C. P.; Garreau, D.; Hapiot, P.; Pinson, J.; Savéant, J. M. *J. Electroanal. Chem.* **1988**, *243*, 321.
(7) Andrieux, C. P.; Garreau, D.; Hapiot, P.; Savéant, J. M. *J. Electroanal. Chem.* **1988**, *248*, 447.
(8) Amatore, C.; Kelly, R. S.; Dristensen, E. W.; Kuhr, W. G.; Wightman, R. M. *J. Electroanal. Chem.* **1988**, *213*, 31.
(9) Ponchon, J.-L.; Cespuglio, R.; Gonon, F.; Jouvet, M.; Pujol, J.-F. *Anal. Chem.* **1979**, *51*, 1483.
(10) Geng, L.; Murray, R. W. *Inorg. Chem.* **1988**, *25*, 3115.
(11) Janata, J.; Bezegh, A. *Anal. Chem.* **1988**, *60*, 62R.
(12) Ikeriyama, Y.; Yamauchi, S.; Yukiashi, T.; Ushioda, H. *Anal. Lett.* **1987**, *20*, 1791.
(13) Ikeriyama, Y.; Yamauchi, S.; Yukiashi, T.; Ushioda, H. *Anal. Lett.* **1987**, *20*, 1407.
(14) Brina, R.; Pons, S.; Fleischmann, M. *J. Electroanal. Chem.* **1988**, *244*, 81.
(15) Childsey, C. E.; Feldman, B. J.; Lundgren, C.; Murray, R. W. *Anal. Chem.* **1988**, *58*, 601.
(16) Murakami, T.; Nakamoto, S.; Kimura, J.; Kuriyama, T.; Karube, I. *Anal. Lett.* **1986**, *19*, 1973.
(17) White, H. S.; Kittlesen, G. P.; Wrighton, M. S. *J. Am. Chem. Soc.* **1984**, *106*, 5375.
(18) Kittlesen, G. P.; White, H. S.; Wrighton, M. S. *J. Am. Chem. Soc.* **1984**, *105*, 7389.
(19) Paul, E. W.; Ricco, A. J.; Wrighton, M. S. *J. Phys. Chem.* **1985**, *89*, 1441.
(20) Thackeray, J. W.; White, H. S.; Wrighton, M. S. *J. Phys. Chem.* **1985**, *89*, 5133.
(21) Bélanger, D.; Wrighton, M. S. *Anal. Chem.* **1987**, *59*, 1426.
(22) Natan, M. J.; Mallouk, T. E.; Wrighton, M. S. *J. Phys. Chem.* **1987**, *91*, 648.
(23) Natan, M. J.; Bélanger, D.; Carpenter, M. K.; Wrighton, M. S. *J. Phys. Chem.* **1987**, *91*, 1834.
(24) Jones, E. T. T.; Chyan, O. M.; Wrighton, M. S. *J. Am. Chem. Soc.* **1987**, *109*, 5526.
(25) Sanderson, D. G.; Anderson, L. B. *Anal. Chem.* **1985**, *57*, 2388.
(26) Bard, A. J.; Crayston, J. A.; Kittlesen, G. P.; Shea, T. V.; Wrighton, M. S. *Anal. Chem.* **1986**, *58*, 2321.
(27) Shea, T. V.; Bard, A. J. *Anal. Chem.* **1987**, *59*, 2101.
(28) Lichi, S.; Cammarata, V.; Wrighton, M. S. *Science* **1988**, *243*, 1176.
(29) Feldman, B. J.; Feldberg, S. W.; Murray, R. W. *J. Phys. Chem.* **1987**, *91*, 6558.
(30) Aoki, K.; Morita, M.; Niwa, O.; Tabei, H. *J. Electroanal. Chem.* **1988**, *256*, 269.
(31) Morita, M.; Longmire, M. L.; Murray, R. W. *Anal. Chem.* **1988**, *60*, 2770.
(32) Aoki, K.; Tokuda, K.; Matsuda, H. *J. Electroanal. Chem.* **1987**, *225*, 19.
(33) Aoki, K.; Tokuda, K.; Matsuda, H. *J. Electroanal. Chem.* **1987**, *230*, 61.
(34) Coen, S.; Cope, D. K.; Tallman, D. E. *J. Electroanal. Chem.* **1988**, *215*, 29.

RECEIVED for review August 14, 1989. Accepted November 29, 1989.

Mediated, Anaerobic Voltammetry of Sulfite Oxidase

L. A. Coury, Jr., B. N. Oliver,[1] J. O. Egekeze,[2] C. S. Sosnoff, J. C. Brumfield, R. P. Buck, and R. W. Murray*

Venable and Kenan Laboratories of Chemistry, University of North Carolina at Chapel Hill, Chapel Hill, North Carolina 27599-3290

The anaerobic voltammetry of the Mo/Fe enzyme, sulfite oxidase (SO), is described for the mediators cytochrome *c*, $[Ru(NH_3)_6]^{3+/2+}$, $TMPD^{+/0}$, and $[Co(bpy)_3]^{3+/2+}$. Theory derived for steady-state voltammetric catalysis correctly predicts the observed concentration and scan-rate dependencies of the catalytic waves. The instances for which existing EC_{cat} theories may be applied to two catalytic reactions coupled to an interfacial charge transfer are considered. The bimolecular rate constant for the reaction of $[Co(bpy)_3]^{3+}$ with reduced SO is calculated and determined to be approximately 5×10^4 L·mol^{-1}·s^{-1}. The appearance of catalytic prepeaks at low sulfite concentrations is noted and the shape of corresponding *i/t* curves from chronoamperometry is examined. The analytical implications of the novel time dependence of the catalytic current under these conditions are discussed.

INTRODUCTION

Increasing interest in electrochemical sensors capable of selective response to species of analytical importance has motivated evaluation of various enzyme systems as sensor components (*1–3*). Perhaps the most widely studied enzymes for this application are the oxidase enzymes (*4*). Under aerobic conditions, many oxidase enzyme-based sensors seek to amperometrically monitor hydrogen peroxide generated from the reduction of dioxygen during the enzymatic reaction sequence.

Recently, ferrocene derivatives have been explored as synthetic electron acceptors for some oxidase enzymes under anaerobic conditions (*5–7*). Electron transfer mediators often offer the advantage of driving enzyme turnover at less extreme potentials than would otherwise [illegible] peroxide were the species to be monitored electrometrically. Decreased operating potentials may increase selectivity by eliminating contributions to the measured response from other species undergoing redox reactions at more extreme potentials. In addition, mediators allow experiments under anaerobic conditions, circumventing problems arising from direct (nonenzymatic) oxidation of the enzymatic substrate by dissolved oxygen.

The enzyme sulfite oxidase [EC 1.8.2.1] has previously been incorporated into membranes and used in Clark-type oxygen electrode based sensors (*8, 9*). There are several disadvantages of the previous approaches. In order to oxidize enzymatically generated peroxide at an appreciable rate, it is necessary to polarize the working electrode at highly positive potentials, where sulfite may itself be oxidized directly. Oxidation of sulfite can lead to passivation of solid electrode surfaces, limiting their useful lifetime (*10*).

For sulfite sensor work, it is common to stabilize aqueous sulfite solutions from air oxidation by adding formaldehyde or glycerol as stabilizers (*8, 11*) to the analyte solution. These stabilizers form adducts with sulfite that are not oxygen sensitive (*12*), thus overcoming the inherent contradiction of employing analyte solutions containing readily oxidizable sulfite but yet saturated with oxygen. Such sensing strategies rely on dissociation of these adducts to supply sulfite for the

[1] Current address: British Gas, London Research Station, Fulham, London, UK SW6 2AD.
[2] Permanent address: Department of Chemistry and Physics, Augusta College, Augusta, GA 30910.
* Author to whom correspondence should be addressed.

0003-2700/90/0362-0452$02.50/0